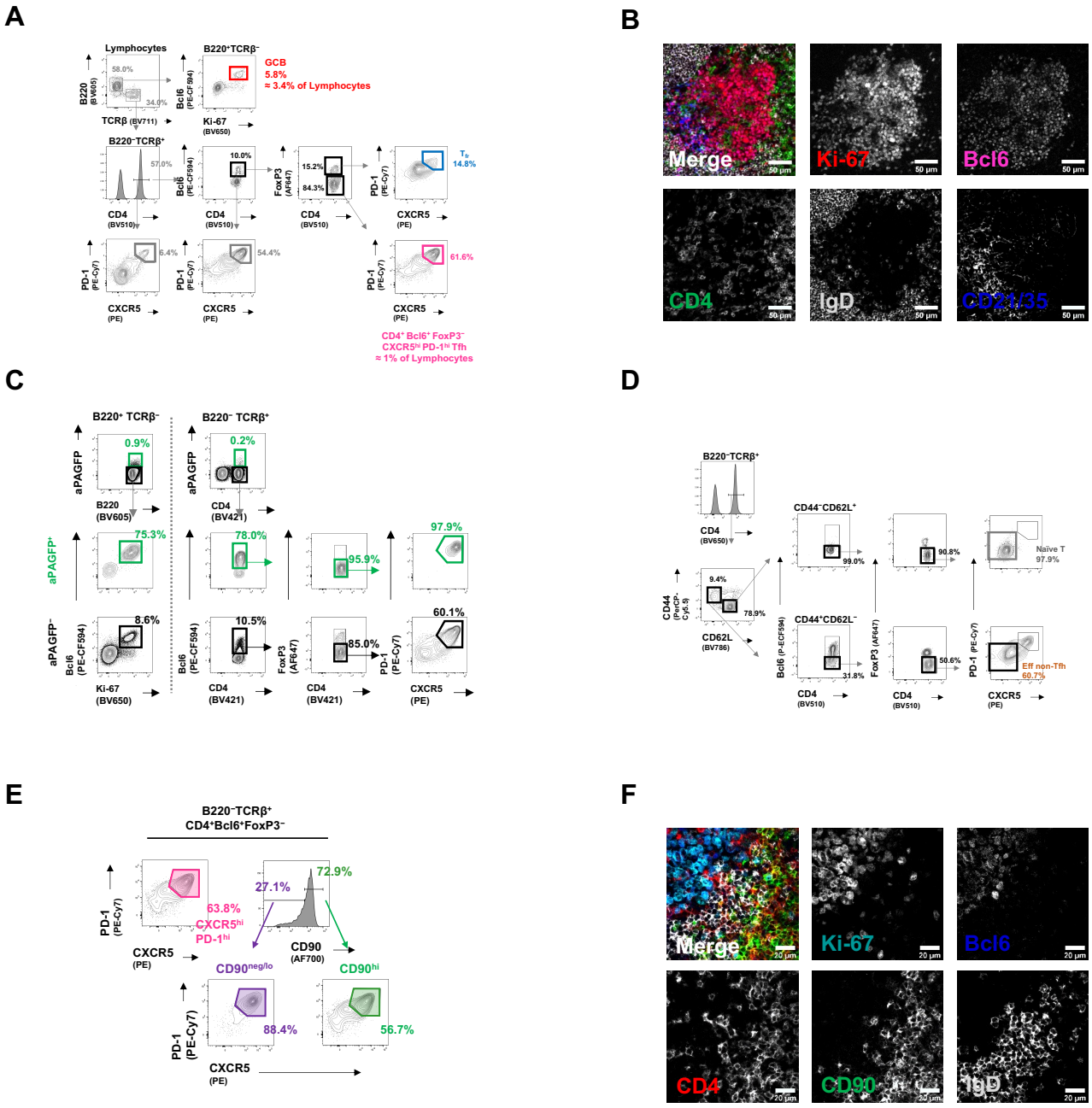

Supplementary Figure 1. Gating strategies to identify GC B cells and GCTfh cells (related to Figure 1). (A-B) B6 mice were immunized as described in **Fig. 1A. (A)** Lymphocytes harvested from the pLNs of immunized mice were pre-gated on single lymphocytes using the height, width and area of forward- and side-scatter signal. Dead cells were excluded using LIVE/DEAD™ reagents. GCB (red), GCTfh (magenta) and Tfr (light blue) cells were defined as B220^{+}TCRβ^{-}Bcl6^{+}Ki-67^{+}, B220^{-}TCRβ^{+}CD4^{+}Bcl6^{+}FoxP3^{-}CXCR5^{hi}PD-1^{hi} and B220^{-}TCRβ^{+}CD4^{+}Bcl6^{+}FoxP3^{+}CXCR5^{hi}PD-1^{hi} populations, respectively. The frequencies of GCB and Tfh cells among total harvested live/single lymphocytes are shown. **(B)** Split-channel images of **Fig. 1C**. The upper left panel represents merged signals from the other 5 panels. CD4 (green), CD21/CD35 (blue), IgD (gray), Bcl6 (magenta), Ki-67 (red). Magnification: x200, scale bars 50 μm. **(C)** PAGFP Tg mice were footpad-immunized and treated as described in **Fig. 1E**. Flow cytometry plots depicting the frequencies of GC B cells and Tfh populations among activated PAGFP (aPAGFP)$^{+}$ (green) and aPAGFP^{-} (black) populations. **(D-F)** B6 mice were immunized as in **Fig. 1A** and analyzed at day 8 or 12 p.i. **(D)** Effector non-Tfh (eff non-Tfh; orange) cells were defined as B220^{-}TCRβ^{+}CD4^{+}CD44^{+}CD62L^{-}Bcl6^{-}FoxP3^{-}CXCR5^{low}PD-1^{low}. **(E)** CD90$^{neg/lo}$ GCTfh (purple) and CD90^{hi} GCTfh-like (green) cells were defined as B220^{-}TCRβ^{+}CD4^{+}Bcl6^{+}FoxP3^{-}CXCR5^{hi}PD-1^{hi}CD90$^{neg/lo}$ and B220^{-}TCRβ^{+}CD4^{+}Bcl6^{+}FoxP3 $^{-}$CXCR5^{hi}PD-1^{hi}CD90^{hi} populations, respectively. The frequencies of CXCR5^{hi}PD-1^{hi} cells in CD90$^{neg/lo}$ and CD90^{hi} Bcl6^{+}FoxP3^{-} T cells are shown. **(F)** Split channel images of **Fig. 1H**. The upper left panel represents merged signals from the other 5 panels. CD4 (red), CD90 (green), IgD (gray), Bcl6 (blue), Ki-67 (cyan). Magnification: x630, scale bars 20 μm.

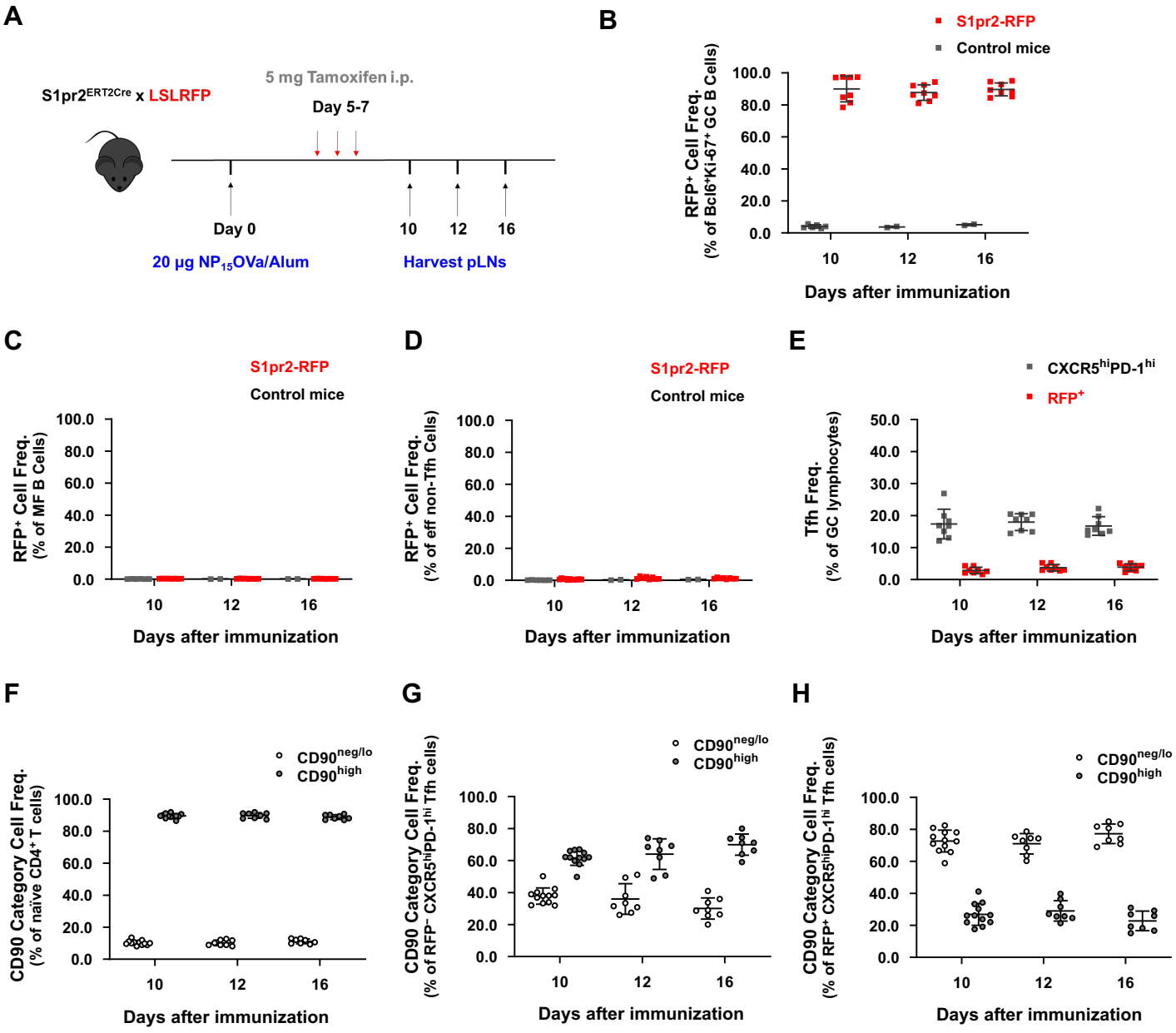

Supplementary Figure 2. Surface CD90 expression is specifically down-regulated on S1pr2-driven RFP-labeled GC-resident Tfh cells (related to Figure 2). S1pr2-RFP mice were footpad-immunized with 20 µg of NP-Ova in alum and treated with 5 mg tamoxifen (*i.p.*) daily at days 5-7 p.i. Draining pLNs were harvested at days 10, 12 and 16 p.i. **(A)** Diagram of the experimental design. **(B-D)** Frequencies of RFP$^+$ cells among **(B)** GCB, **(C)** Mature follicular B cells and **(D)** eff non-Tfh cells (n = 8; mean ± S.D.). **(E)** Frequencies of RFP-marked (red) or all CXCR5^{hi}PD-1^{hi} Tfh cells (black) in the GCs of individual pLNs (n = 8; mean ± S.D.). **(F-H)** Frequencies of CD90^{hi} or CD90$^{neg/lo}$ cells among **(F)** naïve CD4$^+$ T cells, **(G)** RFP$^-$ and **(H)** RFP$^+$ CXCR5^{hi}PD-1^{hi} Tfh cells at indicated time points. Each symbol represents an individual mouse. Data were pooled from ≥2 independent experiments.

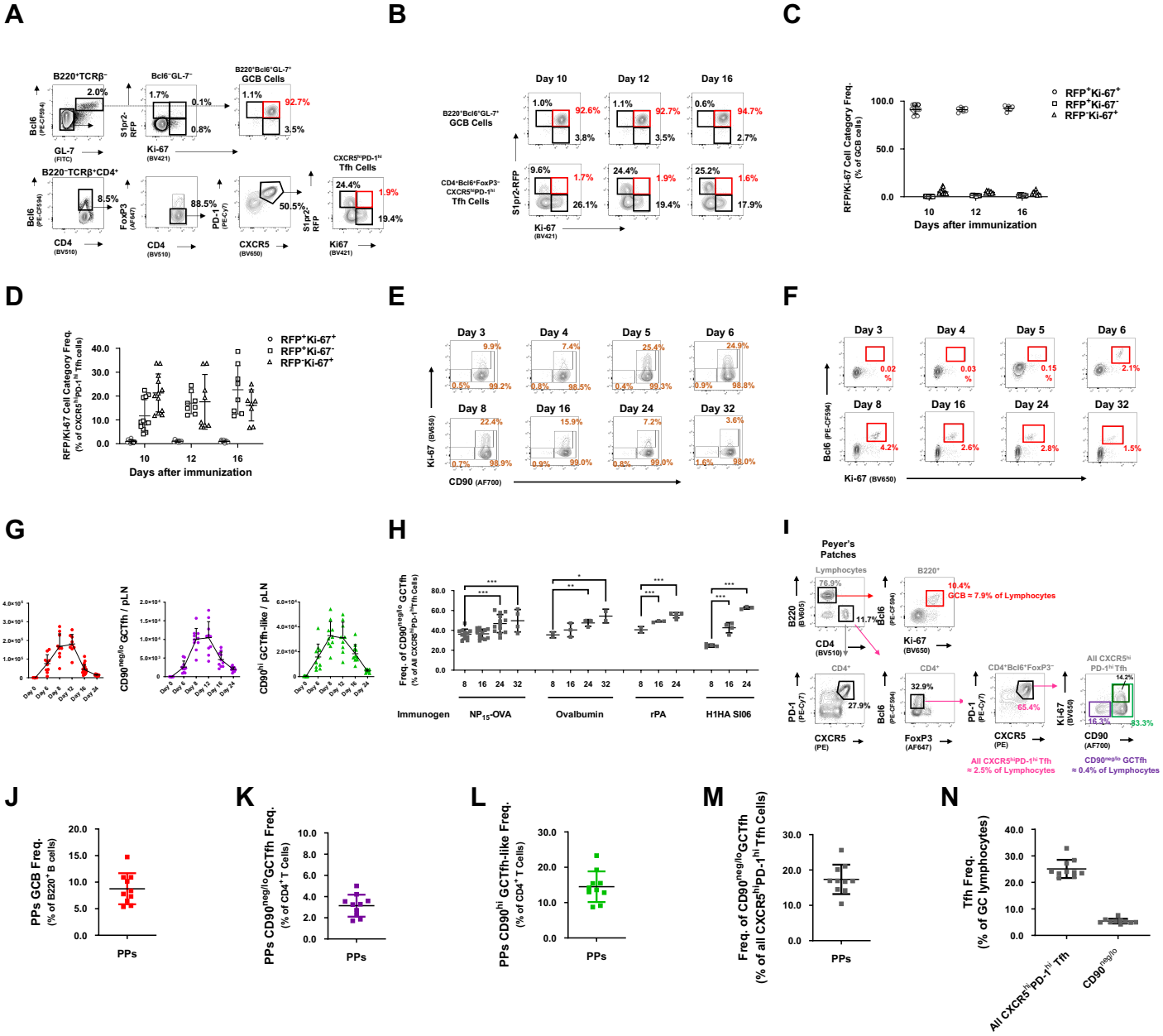

Supplementary Figure 3. GC-resident Tfh cells cease proliferating after GC organization (related to Figure 3). S1pr2-RFP mice were immunized and treated as described in **Fig. S2A.** **(A)** GCB and Tfh cells were defined as B220$^+$TCRβ$^-$Bcl6$^+$GL7$^+$ and B220$^-$TCRβ$^+$CD4$^+$Bcl6$^+$FoxP3$^-$CXCR5^{hi}PD-1^{hi} populations, respectively. The frequencies of RFP$^+$ and Ki-67$^+$ GCB and CXCR5^{hi}PD-1^{hi} Tfh cells are shown. **(B)** Representative flow contour plots showing the frequencies of RFP$^+$Ki-67$^+$, RFP$^+$Ki-67$^-$ and RFP$^-$Ki-67$^+$ cells among GCB and CXCR5^{hi}PD-1^{hi} Tfh cells at indicated time points. **(C-D)** Frequencies of RFP$^+$Ki-67$^+$ (circle), RFP$^+$Ki-67$^-$ (square), and RFP$^-$Ki-67$^+$ (triangle) cells among **(C)** GCB and **(D)** CXCR5^{hi}PD-1^{hi} Tfh cells at indicated time points (n = 8 at each time point; mean ±S.D.). **(E-G)** C57BL/6 mice were immunized and tissues were harvested as described in **Fig. 1A.** **(E)** Representative flow contour plots showing the frequencies of CD90$^{neg/lo}$Ki-67$^-$, CD90^{hi}Ki-67$^+$ (proliferating eff non-Tfh) and CD90^{hi} populations among the eff non-Tfh population in pLNs harvested at indicated time points. Eff non-Tfh were gated as in **Fig. S1D**. **(F)** Representative flow contour plots showing the frequencies of Bcl6$^+$Ki-67$^+$ GCB cells among B220$^+$TCRβ$^-$ total B cells at indicated time points. **(G)** The population kinetics (numbers) of GCB cells (red circle), CD90^{hi} GCTfh-like cells (green triangle) and CD90$^{neg/lo}$ GCTfh cells (purple hexagon) after immunization (n = 10 at each time point; mean ± S.D.). **(H)** B6 mice were immunized with 20 μg of either NP_{15}-Ova, Ova, rPA or rHA in alum, and pLN cells were analyzed at indicated time points. Shown are frequencies of CD90$^{neg/lo}$ GCTfh cells among all CXCR5^{hi}PD-1^{hi} Tfh populations in immunized pLNs (n > 3 at each time point; mean ± S.D.). **(I-N)** PPs from the small intestine of C57BL/6 mice were harvested, stained and subjected to flow cytometric analysis. **(I)** Representative flow plots show the frequency of GCB (red) among total lymphocytes and the frequencies of CD90$^{neg/lo}$Ki-67$^-$ (CD90$^{neg/lo}$ GCTfh; purple), CD90^{hi}Ki-67$^+$ (proliferating GCTfh-like; black) and CD90^{hi} GCTfh-like (light green) populations among all CD4$^+$Bcl6$^+$FoxP3$^-$CXCR5^{hi}PD-1^{hi} Tfh cells in PPs. **(J-L)** Frequencies of PP **(J)** GCB cells, **(K)** CD90$^{neg/lo}$ GCTfh cells and **(L)** CD90^{hi} GCTfh-like cells. **(M)** Frequencies of PP CD90$^{neg/lo}$ GCTfh cells among all CXCR5^{hi}PD-1^{hi} Tfh cells. **(N)** Frequencies of all CXCR5^{hi}PD-1^{hi} Tfh and CD90$^{neg/lo}$ GCTfh in GC lymphocytes (GCB + indicated Tfh) of harvested PPs (n = 10; mean ±S.D.). **(O)** FoxP3^{EGFP} mice were footpad-immunized with 20 μg of NP-Ova in alum. CD90$^{neg/lo}$ GCTfh (purple) and CD90^{hi} GCTfh-like cells (green) were sorted from the same pLN at indicated time points and were subjected to high-throughput TCRβ sequencing. Venn diagrams show the numbers and frequencies of unique and shared templates (Gray; upper row) or VDJ rearrangements (Black; lower row) between CD90$^{neg/lo}$ GCTfh and CD90^{hi} GCTfh-like subsets. Gating strategies are shown in **Fig. S7A**. Data represent one of two independent experiments. (**C-D, G-H, J-N**) Each symbol represents an individual mouse. Data were pooled from at least two independent experiments. Statistical significance was measured using ordinary ANOVA followed by Dunnett's multiple comparison post-tests against the day 8 group in each immunization (*P<0.05; **P<0.01; *** P<0.001).

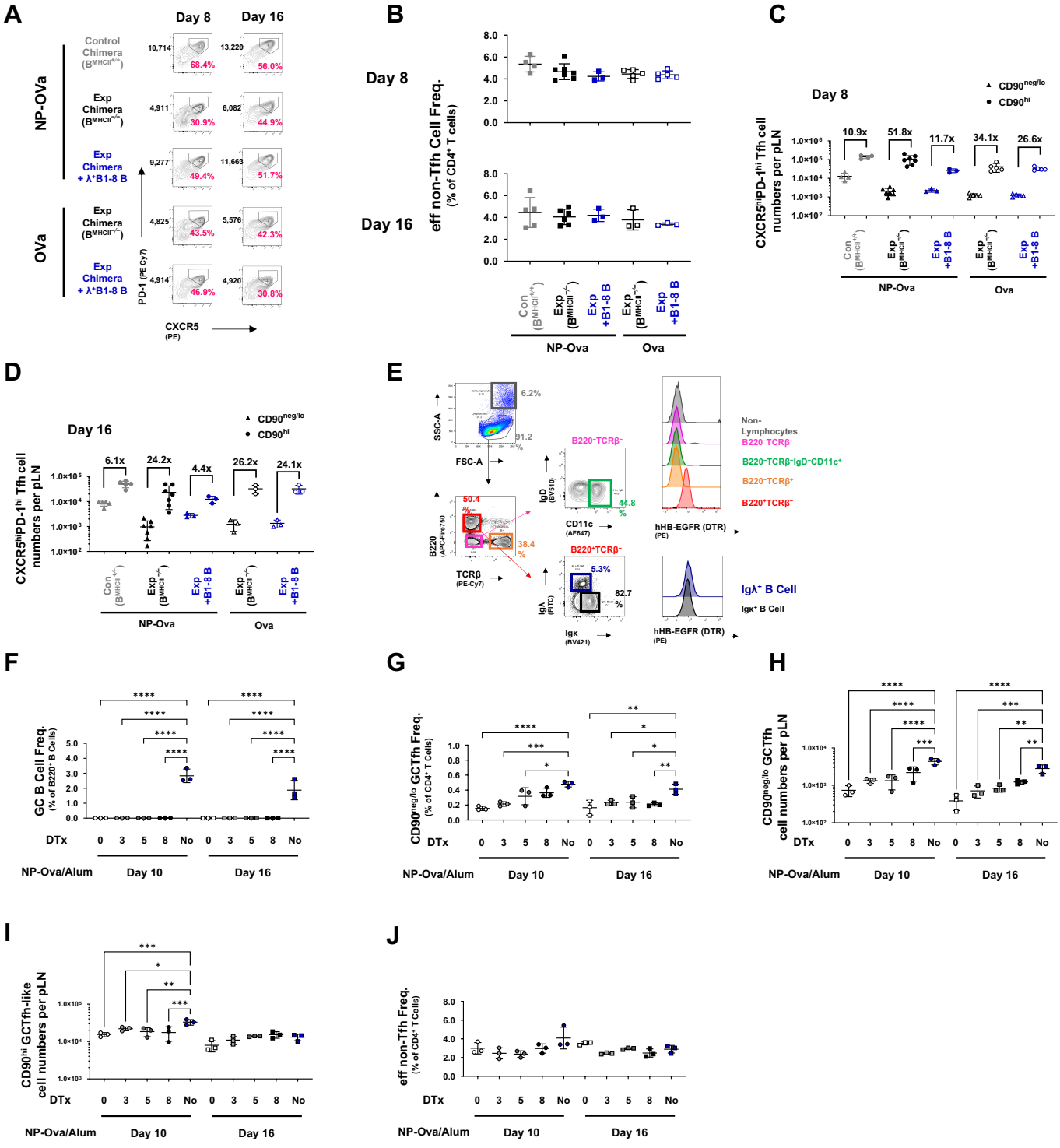

Supplementary Figure 4. CD90$^{neg/lo}$ GCTfh differentiation requires B cells to present cognate pMHCII until GCs completely coalesce (related to Fig. 4 and 5). (A-D) Chimeric mice were generated and treated as described in **Fig. 4A**. **(A)** Representative flow contour plots depicting the frequencies of CXCR5^{hi}PD-1^{hi} cells (magenta) among CD4$^+$Bcl6$^+$FoxP3$^-$ Tfh cells in pLNs at days 8 and 16 p.i. The cross marks the MFI signal within the CXCR5^{hi}PD-1^{hi} gate. Black numbers to the left of each panel denote the PD-1 (PECy7) MFI within the gated population. **(B)** Frequencies of eff non-Tfh cells among CD4$^+$ cells at indicated time points. **(C-D)** absolute numbers of CD90$^{neg/lo}$ GCTfh (triangle) and CD90^{hi} GCTfh-like (circle) cells per pLN at **(C)** day 8 and **(D)** day 16 p.i. (**A-D**; n = 3-8 at each time point; mean ±S.D.). **(E)** Human HB-EGP receptor (diphtheria toxin [DTx] receptor) expression on blood leukocytes from Mb1^{Cre} x DTR^{LSL} mice. The DT receptor was expressed on all B220$^+$ B cells. **(F-J)** Chimeric mice were generated and treated as in **Fig. 5A**. Shown are **(F)** frequencies of GCB cells, **(G)** frequencies of CD90$^{neg/lo}$ GCTfh, **(H)** absolute numbers of CD90$^{neg/lo}$ GCTfh, **(I)** absolute numbers of CD90^{hi} GCTfh-like and **(J)** frequencies of eff non-Tfh in CD4$^+$ cells at indicated time points (**F-J**; n = 3 at each time point; mean ±S.D.). Each symbol represents an individual mouse. Data were pooled from at least two independent experiments. Statistical significance was measured using ordinary ANOVA followed by Tukey's multiple comparison post-tests (***P<0.01; **** P<0.001).

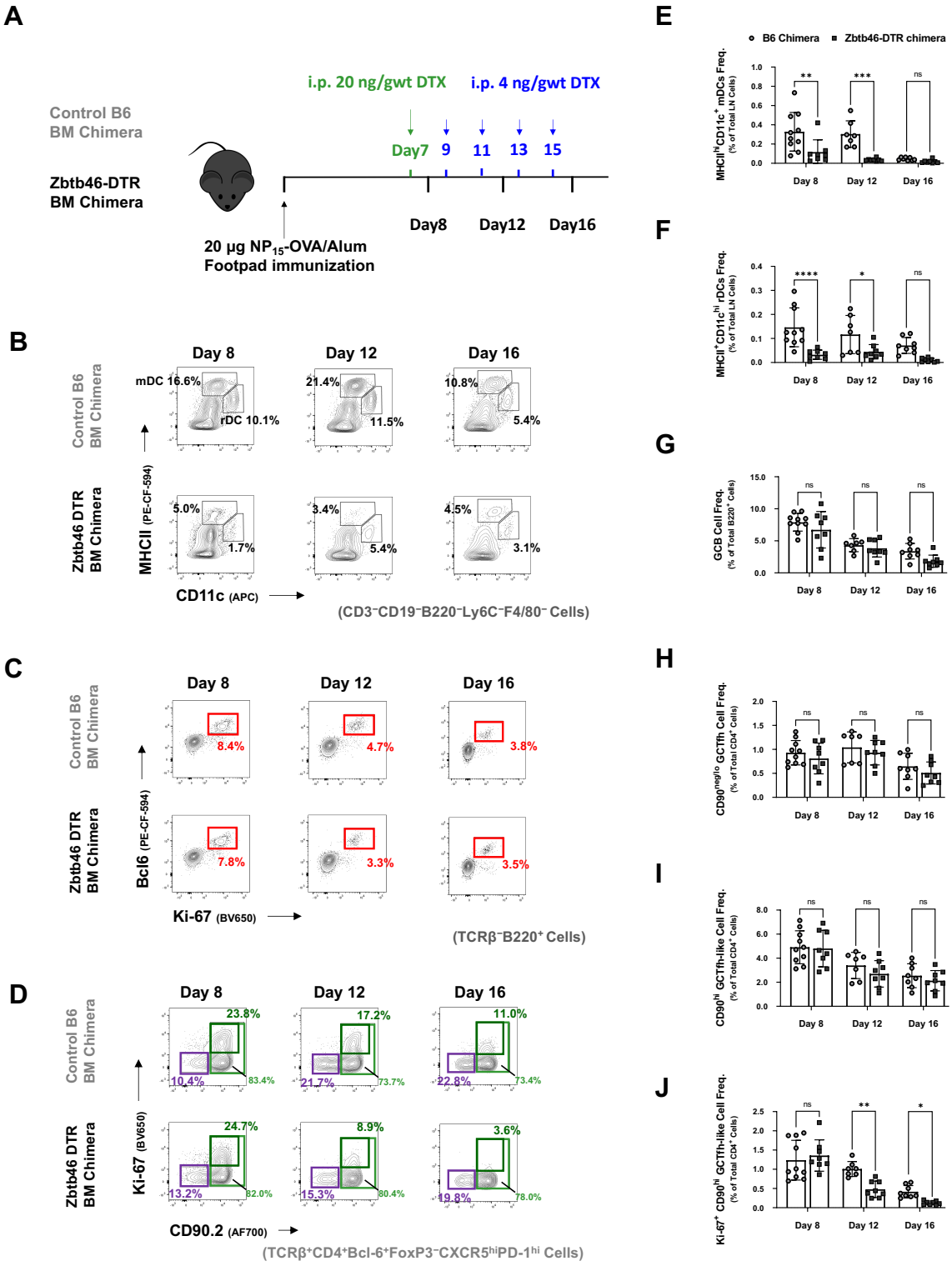

Supplementary Figure 5. Depletion of cDCs during GC responses halt proliferation in CD90^{hi} Tfh-like cells (related to Figure 4 and 5). (A) Diagram of the experimental design. **(B)** Representative flow contour plots showing the frequencies of MHCII^{hi}CD11c^{+} mDCs and MHCII^{+}CD11c^{hi} rDCs among CD3^{-}CD19^{-}B220^{-}Ly6C^{-}F4/80^{-} cells in pLNs at indicated time points. **(C)** Representative flow contour plots showing the frequencies of Bcl6^{+}Ki-67^{+} GCB cells (red) among B220^{+}TCRβ^{-} total B cells in pLNs at indicated time points. **(D)** Representative flow cytometry contour plots depicting the frequencies CD90$^{neg/lo}$ Ki-67^{-} (CD90$^{neg/lo}$ GCTfh; purple), CD90^{hi} GCTfh-like (light green) or Ki-67^{+}CD90^{hi} GCTfh-like (dark green) cells among all CXCR5^{hi}PD-1^{hi} Tfh cells in pLNs at indicated time points. **(E-J)** Frequencies of **(E)** MHCII^{hi}CD11c^{+} mDCs among all pLN cells, **(F)** MHCII^{+}CD11c^{hi} rDCs among all pLN cells, **(G)** GCB cells among total B220^{+} B cells, **(H)** CD90$^{neg/lo}$ GCTfh cells, **(I)** CD90^{hi} GCTfh-like cells and **(J)** Ki-67^{+}CD90^{hi} GCTfh-like cells among all CXCR5^{hi}PD-1^{hi} Tfh cells at indicated time points (n = 7-10 at each time point; mean ±S.D.). Each symbol represents an individual chimera mouse from at least two independent experiments. Statistical significance was measured using two-way ANOVA followed by Sidak's multiple comparison post-tests (*P<0.05; **P<0.01; *** P<0.001, ****P<0.0001).

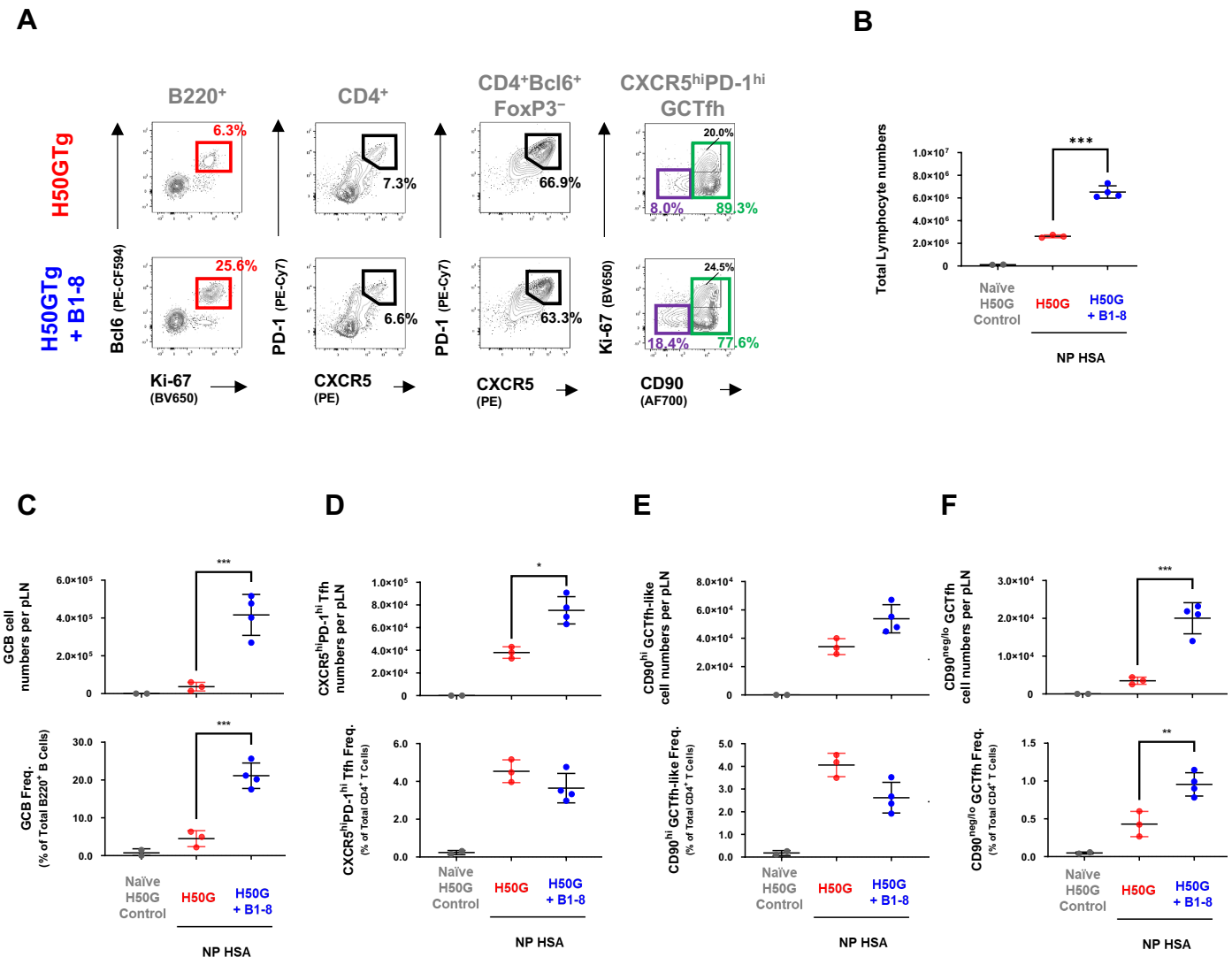

Supplementary Figure 6. Transfer of B1-8 B cells to B6.H50Gμ transgenic mice increases GCB- as well as GC-resident CD90$^{neg/lo}$ GCTfh-responses after NP-immunization (related to Figure 6). Recipient B6.H50Gμ transgenic mice injected with PBS (control) or 1 x 10^5 NP$^+$ B1-8i mature follicular B cells (experiment) were immunized with 20 μg of NP-HSA in alum via footpad. pLN lymphocytes were harvested, stained and examined by flow cytometry 8 days p.i. **(A)** Representative flow contour plots showing the frequencies of B220$^+$Bcl6$^+$Ki-67$^+$ GC B cells (red; far left panel), all CD4$^+$CXCR5^{hi}PD-1^{hi} Tfh cells (left panel), CD4$^+$Bcl6$^+$FoxP3$^-$CXCR5^{hi}PD-1^{hi} GCTfh cells (right panel) and the frequencies of CD90$^{neg/lo}$Ki-67$^-$ (CD90$^{neg/lo}$ GCTfh; purple), CD90^{hi}Ki-67$^+$ (proliferating GCTfh-like; black) and CD90^{hi} GCTfh-like (green) populations in pLNs harvested from control and experiment mice at day 8 p.i. **(B-F)** Absolute numbers and frequencies of **(B)** lymphocytes, **(C)** GCB cells, **(D)** all CXCR5^{hi}PD-1^{hi} Tfh cells, **(E)** CD90^{hi}GCTfh-like cells and **(F)** CD90$^{neg/lo}$ GCTfh cells at day 8 p.i. (n = 3-4; mean ±S.D.). Each symbol represents an individual mouse. Results pooled from at least two independent experiments. Statistical significance was measured using ordinary ANOVA followed by Tukey's multiple comparison post-tests (*P<0.05; **P<0.01; *** P<0.001).

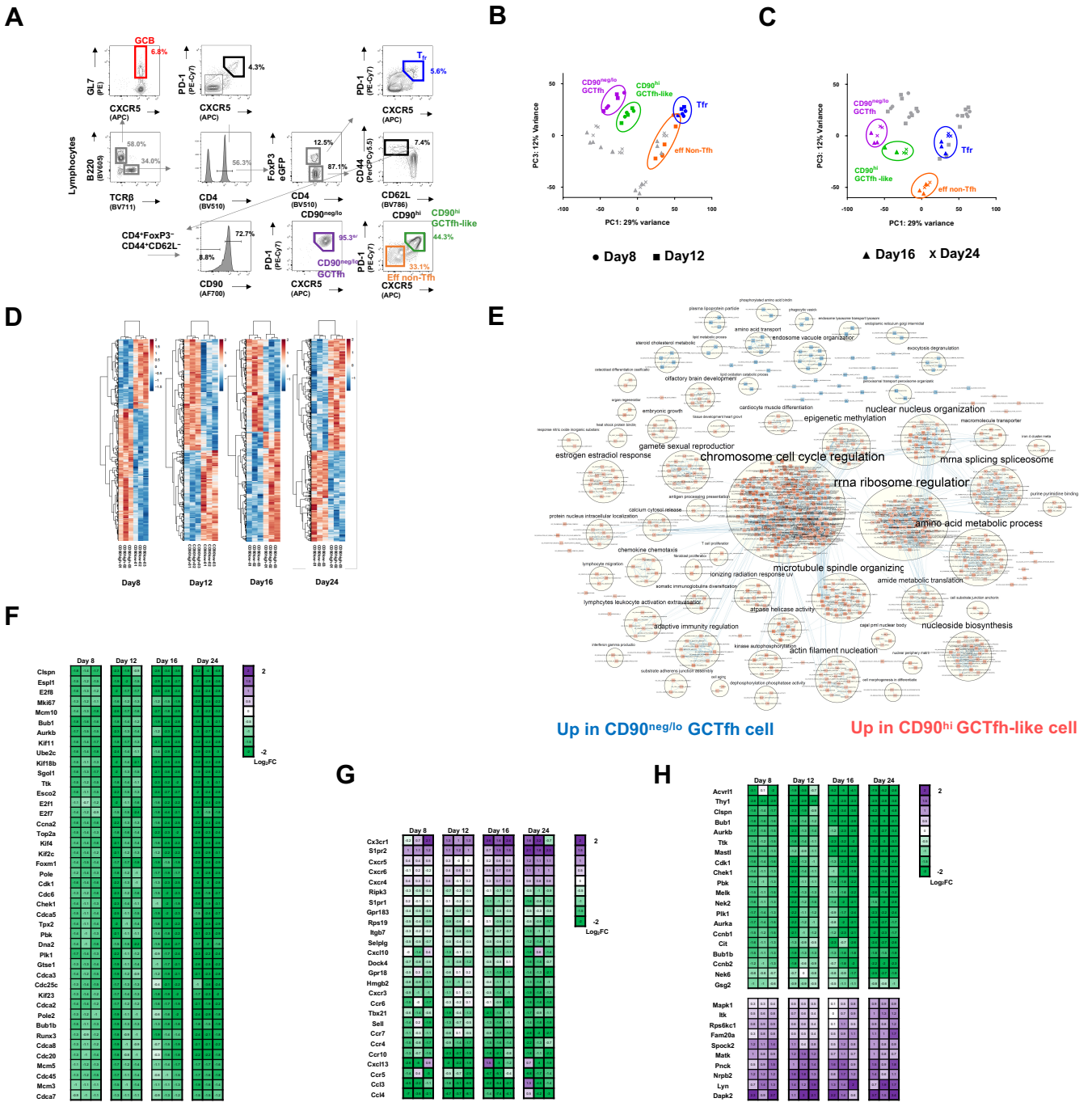

Supplementary Figure 7. CD90$^{neg/lo}$ GCTfh and CD90^{hi} GCTfh-like cells are phenotypically similar but functionally and physiologically divergent populations (related to Figure 7). FoxP3^{EGFP} mice were footpad-immunized with 20 µg of NP-OVA in alum and harvested at days 8, 12, 16 and 24 p.i. CD90$^{neg/lo}$ GCTfh (purple) and CD90^{hi} GCTfh-like (green) cells were sorted from the same pLN and subjected to ultra-low RNA sequencing. **(A)** CD90^{low}GCTfh (purple), CD90^{hi}GCTfh-like (green), eff Non-Tfh (orange) and Tfr (light blue) cells were sorted as B220$^-$TCRβ$^+$CD44$^+$CD62L$^-$FoxP3$^-$CD90^{low}CXCR5^{hi}PD-1^{hi}, B220$^-$TCRβ$^+$ CD44$^+$CD62L$^-$FoxP3$^-$ CD90^{hi}CXCR5^{hi}PD-1^{hi}, B220$^-$TCRβ$^+$CD44$^+$CD62L$^-$FoxP3$^-$CD90^{hi}CXCR5^{low}PD-1^{low} and B220$^-$TCRβ$^+$CD44$^+$CD62L$^-$FoxP3$^+$CXCR5^{hi}PD-1^{hi} populations, respectively. **(B)** Principal components analysis of day 8 and day 12 samples. **(C)** Principal components analysis of day 16 and day 24 samples. **(D)** Heatmap graph representing differentially expressed genes in GCTfh and Tfh-like cells at indicated time points (P < 0.05 & ≥ 2-fold-change for each comparison). Gene expression was z-score normalized and the samples and genes were clustered by correlation distance with complete linkage. **(E)** Gene set enrichment analysis was performed to identify gene ontology terms with altered gene expression for each of the comparisons performed. Significant gene sets with FDR < 0.1 or P < 0.01 were visualized with Cytoscape and Enrichment Map. GSEA Enrichment results were mapped as a network of gene sets (nodes) related by mutual overlap (edges), where the color intensity represents significance and color hue represents the class of interest (that is, enriched in CD90$^{neg/lo}$ GCTfh, blue; enriched in CD90^{hi}GCTfh-like, red). Groups of gene set comparison nodes with overlapped gene list (Overlap coefficient >0.375) are circled and labeled with AutoAnnotate 1.3 using clusterMaker 2. **(F-H)** Heatmap graph showing the fold-change of **(F)** cell division- and proliferation-, **(G)** chemotaxis- and cell migration- and **(H)** protein kinase phosphorylation-related gene expression in CD90$^{neg/lo}$ GCTfh over CD90^{hi}GCTfh-like cells in each individual pLN. Numbers indicate the value of $\log_2$ fold-change in gene expression in each sample (n = 3 at each time point).